Chapter 5

b) Ag-Based Magnetic Metal Organic Framework Nanocomposite as Catalyst for Nitrophenol Removal

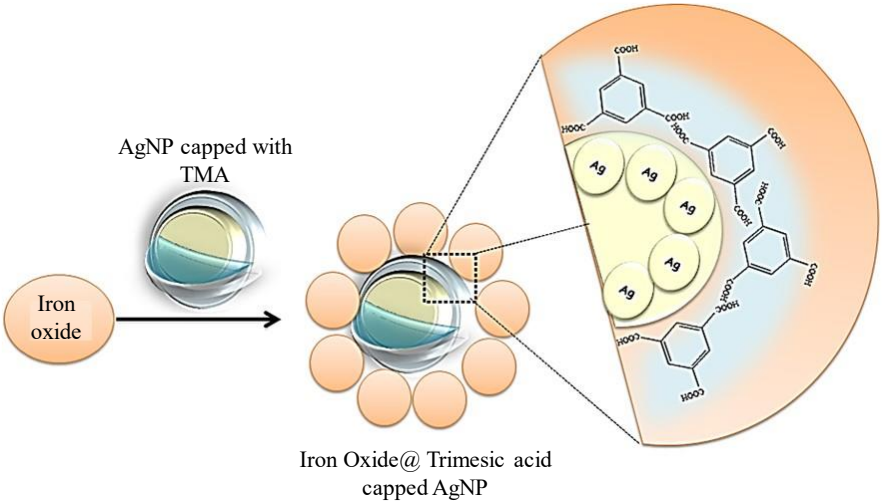

5b.1 Introduction

Metal-organic frameworks (MOFs) are porous, crystalline substances created by coordinating metal ions with organic ligands. Due to their larger specific surface areas, simplicity in separation, higher porosity, variety of structures and functions, they have gained a lot of attention. MOFs constructed from a variety of organic binding ligands and metal ions have made it possible to more systematically engineer their chemical and physical characteristics, making them useful for a variety of applications in various fields, such as gas adsorption and separation, sensors, drug delivery, catalysis or other areas (Zhao et al., 2015) (figure 5b.1)**.** An external magnetic field can be used to quickly separate magnetic Fe_3O_4 from reaction fluids. Magnetic MOF composites, which are made of MOFs and magnetic nanoparticles, have great benefits in adsorption and separation.

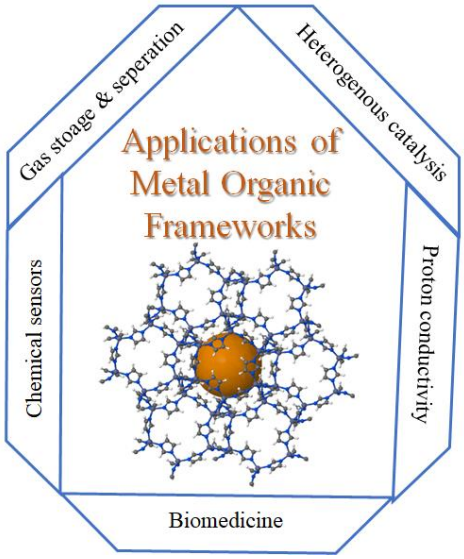

Figure 5b. 1. Application of metal organic frameworks

Immobilizing AgNPs/nanofluids onto a support provided a practical way to address reusability issues while maintaining the catalysts' high catalytic activity and reusability (Xianchun Liu et al., 2015)(Q. Mao et al., 2015). The catalytically active metal NPs have also been immobilized on solid supports with mesopores like SBA-15 (X. Zhang et al., 2013) and MCM-41 (D. Chen et al., 2013)(Selvakannan et al., 2013) in order to control their catalytic properties which have been regarded as ideal supports for heterogeneous catalysis due to their excellent stability, high surface area, tunable pore size and robust surface chemistry. Naik et al. reported the production of AgNP within the pores of Mesoporous silicas (like SBA-15) (Naik et al., 2011) and mesoporous alumina for the conversion of 4-NP to 4-AP (Naik et al., 2012).

Dong et al. synthesized silver nanoparticles immobilized on fibrous nano- for reduction of 4-nitrophenol and 2-nitroaniline (Dong et al., 2014).

Liu and co. studied the catalytic potential of an Ag NPs/Si chip for nitro aromatics reduction (Xiang Liu et al., 2014).

Magnetic metal organic framework nanocomposites (MMOFCs) fabricated by hybridization of magnetic nanoparticles and metal organic frameworks (MOFs), possess the structure and performance of MOFs as well as magnetic properties that can help in their separation and recyclability. MMOFCs have thus gained attention as candidates with great potential for environmental remediation as sorbents and solid phase extractants that can be effectively separated by means of an external magnetic field and reused (Meteku et al., 2020).

Specifically, iron-based MOFs, such as Fe-benzene tricarboxylic acid, Fe-BTC commercially called as BasoliteS F300, have been used as catalyst supports (Rivera-Torrente et al., 2018), as catalyst for quinazolinone synthesis (Oveisi et al., 2016) and as photocatalyst for degradation of dyes (Hossein Zadeh et al., 2019). Iron oxide has been used as support for impregnating Ag nanoclusters (Islam et al., 2016) with potential for catalytic hydrogenation of 4-nitroaniline. Ag-based nanocomposites, have been extensively investigated as catalysts because of their high activity, easy preparation, low cost, good stability and low toxicity.

U. Kurtan et al. synthesized magnetically recyclable $MnFe_2O_4$@SiO_2@Ag nano catalyst for the catalytic reduction of azo dye and nitro compounds (Kurtan et al., 2016). This magnetic nano catalyst has been observed to have excellent reusability properties that remained constant even after several cycles.

Pratik Nariya et al. developed recyclable magnetic silver cyclodextrin nanocomposite with catalytic potential for simultaneous reduction of nitroaromatics and organic dyes from waste water (Nariya et al., 2020).

Thanh-Danh Nguyen used *Jasminium subtriplinerve* to synthesize AgNP which was then capped with nanocomposite 2-hydroxypropyl-β-cyclodextrin/alginate and used for the degradation of pollutants such as 4-nitrophenol, methyl orange and rhodamine B (Nguyen et al., 2018).

Zhengping Dong et al. anchored amino groups on fibrous silica for the well dispersion of silver nanoparticles on it (Dong et al., 2014). The synthesized novel fibrous nano-silica base nano catalyst had been used for the reduction of 4-nirophenol and 2-nitroaniline.

There are several reports available where the metal core shell nanoparticles are used for reduction of nitro compounds. Zhengping Dong et al. modified fibrous silica nanospheres

using Ni@Pd core-shell nanoparticles. The core shell of Ni@Pd NPs possessed a magnetic core of Pd. The catalyst was used for the reduction of 4-nitrophenol.

Shmuel Gonen et al. had prepared Silver Organic Framework of Benzene tricarboxylic acid or trimesic acid incorporated in Activated Carbon(Gonen et al., 2019) and investigated its electrocatalytic activity. Huang et al. prepared a silver based MOF by self-assembly of silver(I) and carboxylate incorporating pyrazine as an auxiliary ligand(Huang et al., 2013). Silver trimesic acid based MOF were fabricated by S. Kamal and T.C.-K. Yang as SERS substrate for detection of organic pollutants(Kamal & Yang, 2021), while Xiu-Ju Yin and Long-Guan Zhu fabricated silver trimesic acid based MOF as a photocatalyst for degradation of methylene blue (Yin & Zhu, 2019).

In the present work, it was decided to take into advantage multiple carboxyl groups of BTC for binding Fe_3O_4 to Ag-BTC to prepare nano IO@Ag-BTC MMOFCs and evaluate its potential as catalyst using nitrophenol reduction as the model reaction.

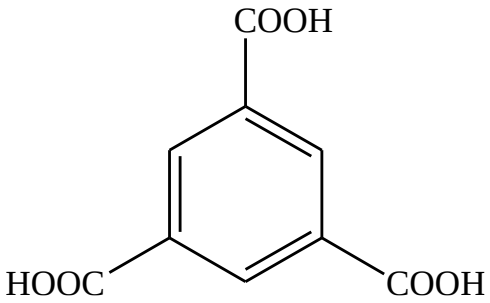

Figure 5b. 2. Structure of Benzene tricarboxylic acid (BTC)

5b.2 Materials and methods

5b.2.1 Materials and Chemicals

Silver nitrate ($AgNO_3$, Spectrochem; 99.9%), Trimesic acid (Sigma aldrich), $FeCl_3$ (Spectrochem), and Ferrous sulphate (Spectrochem) were used in this study without further purification.

5b.2.2 Synthesis of Iron oxide nanoparticles

The iron oxide nanoparticles were synthesised by co-precipitation technique. Briefly, 0.03 M Fe^{2+} and 0.015 M Fe^{3+} were mixed followed by dropwise addition of 1 mL of 0.1 M ammonia solution and stirred for 2-3 minutes. The colour of the solution initially changed to brown and then to black indicating the formation of iron oxide nanoparticles.

5b.2.3 Synthesis of nano Ag-BTC MOFs

For the synthesis of Ag-BTC MOF, 0.03 M BTC solution in NaOH was added dropwise to 50 mL of 0.03 M $AgNO_3$ solution under stirring in 100 mL beaker. The solution turned yellow indicating the formation of Ag-BTC MOF(Ag-BTC).

5b.2.4 Synthesis of IO@Ag-BTC MMOFC

A simple mixing strategy was adopted to synthesize IO@Ag-BTC wherein the Ag-BTC MOF containing solution formed in section 2.3 was added to IO containing solution prepared in section 2.2 under stirring conditions. The mixture was stirred for half an hour and was filtered through Whatman filter paper no. 1 followed by washing several times with water to remove free $AgNO_3$. Finally, it was dried in oven at 100°C.

During the course of this work Chang et al., reported the fabrication of Fe_3O_4@MIL-100(Fe)/Ag and its catalytic potential towards the reduction of nitrophenol (Chang et al., 2020). However, the MOF was fabricated by functionalization of Fe_3O_4 with carboxyl groups followed by formation of Fe_3O_4@MIL-100(Fe) in second step and Fe_3O_4@MIL-100(Fe)/Ag in the third step and irradiation with gamma rays. The resulting MOF was used as catalyst for reduction of nitrophenol.

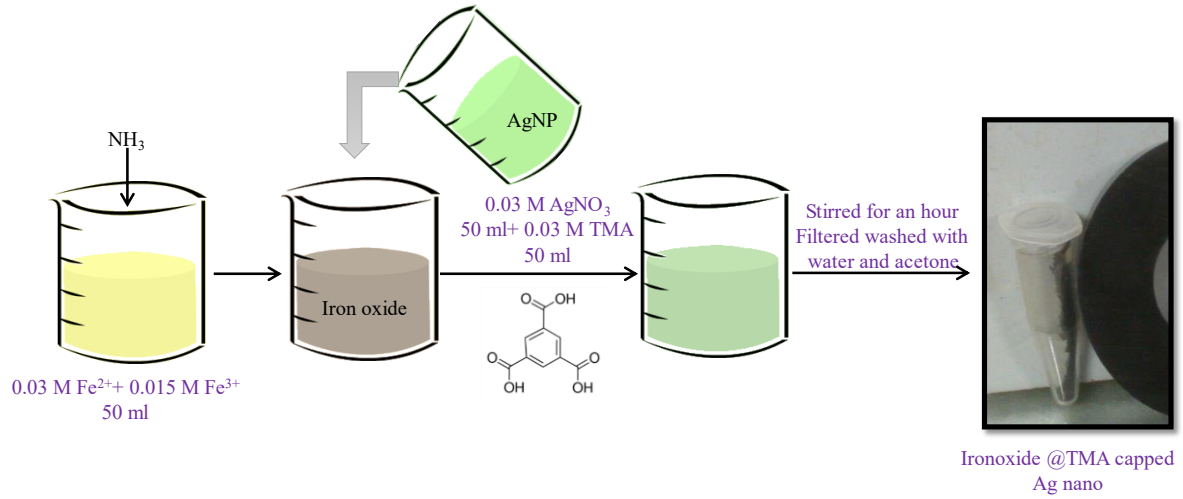

5b.2.5 Catalytic reduction of Nitrophenol

The efficacy of IO@Ag-BTC MMOFC as catalyst was investigated for catalytic reduction of PNP. The reaction was performed by taking 10 mL of 100 ppm of PNP in 25 mL beaker to which 0.2 mL of 0.1 M $NaBH_4$ solution was added under stirring followed by addition of 10 mg of IO@Ag-BTC MMOFC. The reaction mixture was kept under stirring till the solution turned colorless. The reaction was monitored at 1 min interval by withdrawing 0.5mL aliquot of the solution, diluting to 5 mL and measuring the decrease in absorbance at 400nm using a

JASCO-V635 UV- Visible spectrophotometer. After completion of reaction, the catalyst was separated by magnet.

5b.3 Results and discussion

5b.3.1 Characterisation of IO@Ag-BTC MMOFC

UV spectroscopy analysis

The UV-Vis spectra (figure 5b.3a) shows a shoulder band at ~ 250 nm which could be assigned to the characteristic π to π* transition of BTC while the band at 350 nm may be attributed to the 4*d*→5*sp* inter-band transitions of silver nanoclusters embedded in BTC (Islam et al., 2016) and probably to the quadrupole resonance caused due to the presence of low-dimensional non-spherical particles that might have led to non-uniform incidence of light across the sphere. The broad absorption band centred in the region 450-600 nm can be attributed to the d-d transition of Fe^{3+}, as well as transverse band of spherical NPs at 400 - 450 nm and longitudinal plasmon band of Ag nano rods at 600-700 nm (Link & El-Sayed, 1999). The UV-visible absorption bands thus suggest that the solution consists of low symmetry particles and nanorods together with fine nanoclusters (Panda et al., 2018). The EDX spectrum (figure 5b.4a) of IO@Ag-BTC confirmed the presence of iron and silver.

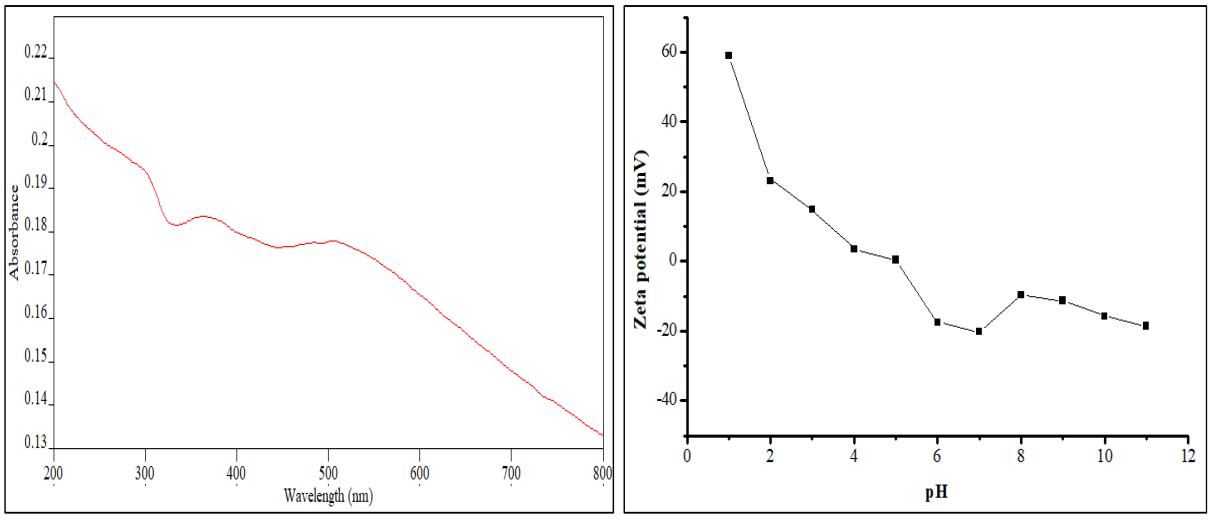

Figure 5b.3 a) UV spectra and b) Zeta potencial of IO@Ag-BTC MMOFC

Transmission electron microscopy

TEM Transmission Electron Micrographs of IO@Ag-BTC nanostructures (figure 5b.4b) with two different contrasts due to presence of silver and iron oxide were observed. The Ag nanoparticles, which have higher Z exhibited darker contrast. A large number of low-symmetry spherical shaped particles of size ~53 nm together with some rod-like shapes

with aspect ratio ranging from 3.7 to 11.23 nm were observed. The SAED pattern of IO@Ag-BTC MMOFC exhibited diffraction rings attributed to (220), (311, 111), (400, 200), (422, 511) and (440, 220) planes iron oxide.

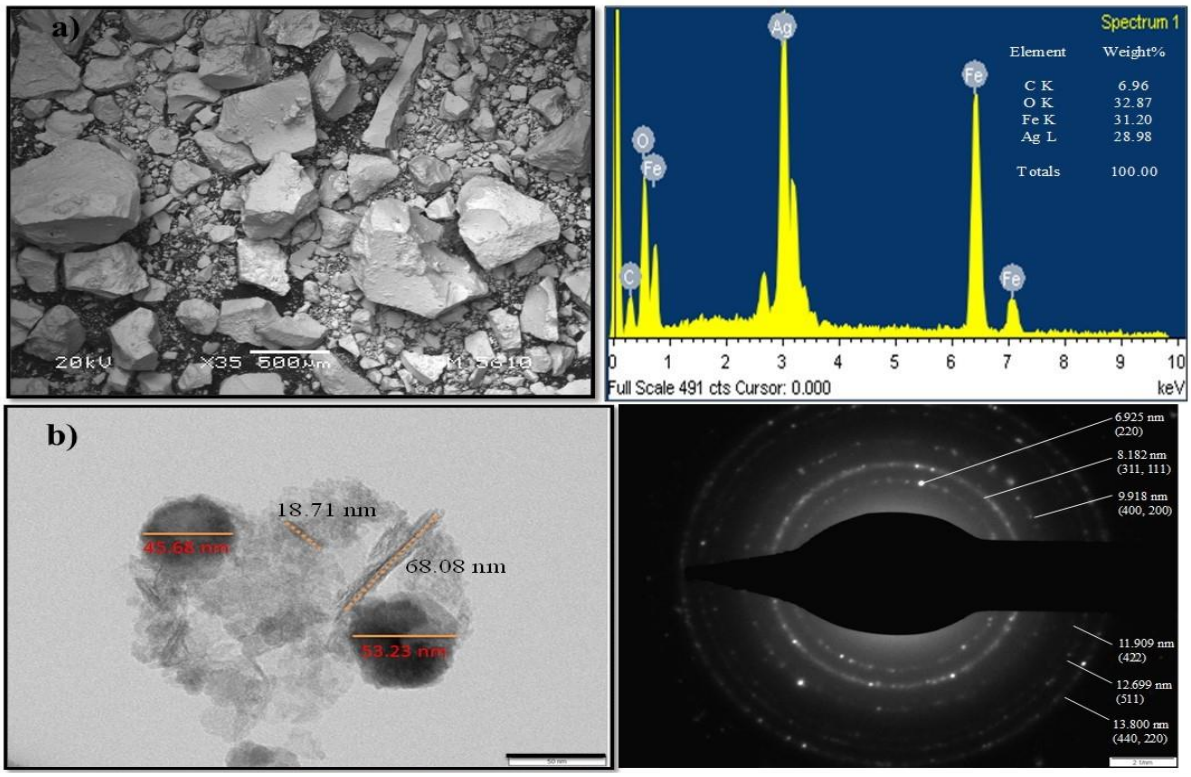

Figure 5b.4 a) EDAX of IO@Ag-BTC MMOFC, b) TEM images of IO@Ag-BTC MMOFC

X-Ray diffraction analysis

The XRD pattern of IO@Ag-BTC MMOFCs is shown in Figure 5b.5. X-ray diffraction peaks of weak intensity at 2θ of 32.14º and 35.5º were related to the diffraction of (220) and (311) planes of Fe_2O_3(maghemite)/Fe_3O_4(magnetite), the diffraction peaks at 2θ 22.84 º and 27.58º peaks were attributed to (210) and (211) planes of maghemite (Ruíz-Baltazar et al., 2015) while the diffraction peaks at 2θ of 38.0º, 44.18º, 64.34º, 77.32º were attributed to (111), (200), (220), (311) diffraction planes of Ag nanoparticles respectively. The prominent diffraction peak at 38º indicated that the preferential longitudinal growth was along the (111) crystal plane during formation of rods of Ag (Rekha et al., 2018). The diffraction peaks of Ag appear to be much stronger than those for Fe_2O_3, indicating that the crystallization of Fe_2O_3 NPs was less ordered as compared to AgNPs.

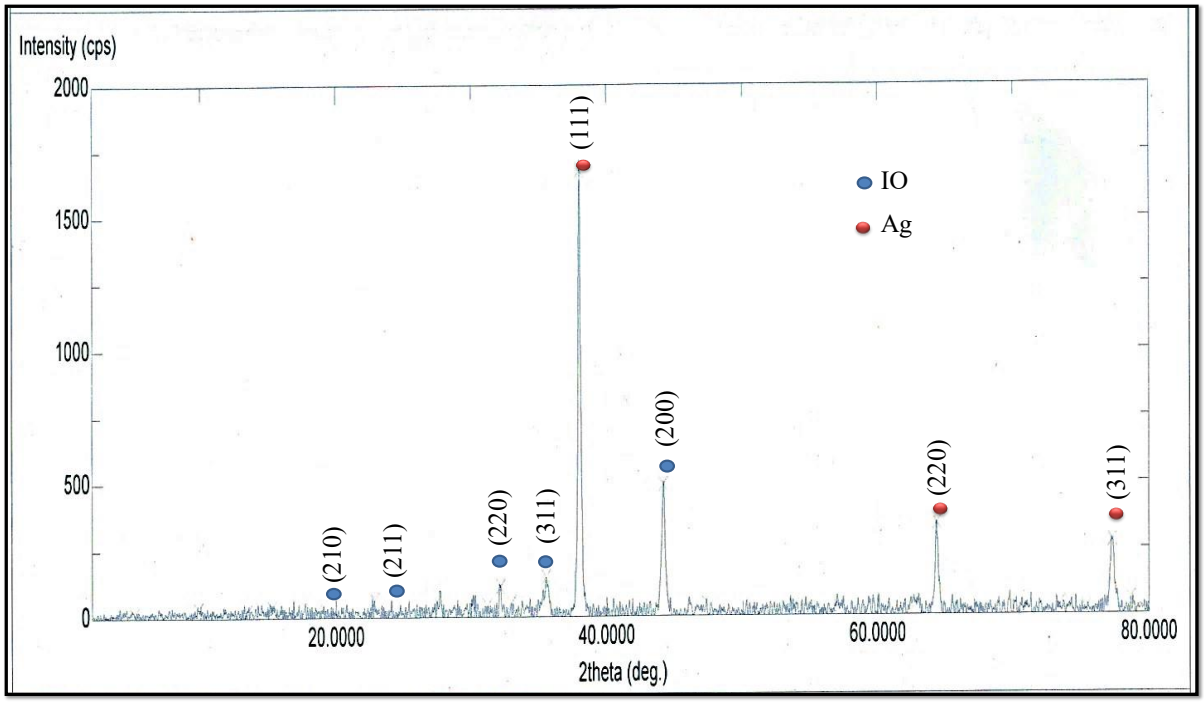

Figure 5b.5 XRD of IO@Ag-BTC MMOFC

FTIR analysis

The IR spectrum of BTC (figure 5b.6) exhibited bands at 1606 cm^{-1} and 1681-1727 cm^{-1} that can be attributed to presence of protonated and deprotonated carboxylic acid groups. The C-H stretching mode of BTC was assigned to the signal at 3090 cm^{-1} while the aromatic C-H in plane bending modes were assigned to the peaks at 1286, 1248, 1180 cm^{-1} and C-H out of plane bending vibration to 919 cm^{-1}. The bands observed at 1327 cm^{-1} and 1402 cm^{-1} were attributed to OH out of plane bending mode of carboxyl group, while the peak at 3350 to 3400 cm^{-1} was attributed to O-H stretching of carboxylic acid group (Mahalakshmi & Balachandran, 2014). The C-C ring stretching vibrations of benzene were observed in the region 1455, 1519 cm^{-1} and 1107, 1180 cm^{-1}. The in-plane and out-of-plane bending vibrations of the benzene ring were observed at 919 cm^{-1}.

The infrared spectrum of pristine iron oxide (figure 5b.6) exhibited vibrational modes that appeared at 3627 cm^{-1}, 2353 cm^{-1}, 3354 cm^{-1} and 1669 cm^{-1} are assigned to the O-H bending vibrations and vibrations of hydrogen-bonded water molecules adsorbed on the surface, while the peaks in the range 400 to 800 cm^{-1} can be attributed to Fe-O vibrations of iron oxide (Daou et al., 2008).

The spectra of Ag-BTC (figure 5b.7) displayed the characteristic carboxylate peaks at about 1553, 1357 cm^{-1}as a result of the delocalized electronic cloud of carboxyl groups confirming the formation of metal organic framework(Wei et al., 2017).

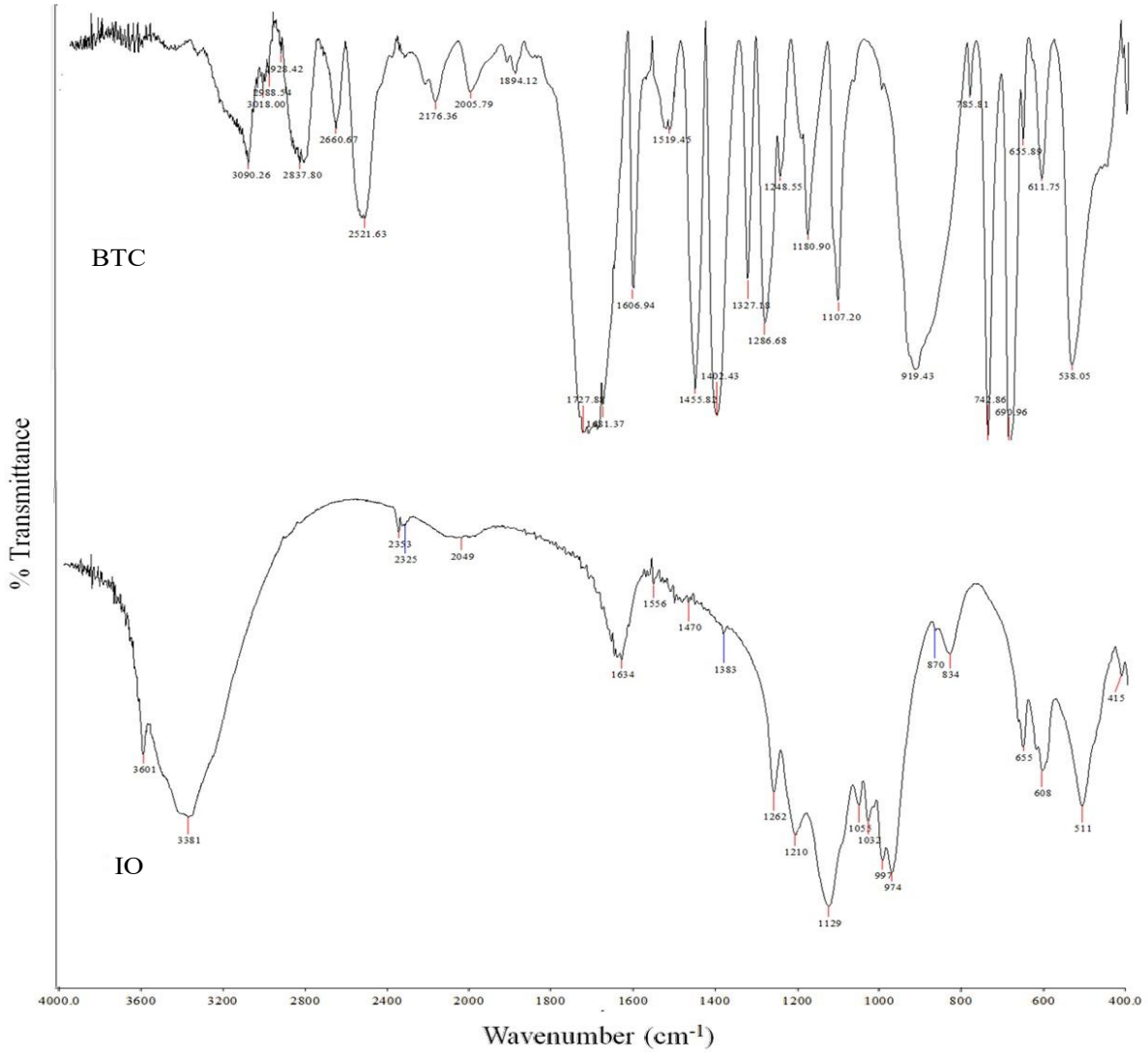

Figure 5b.6 IR spectra of BTC and IO

The spectrum of IO@BTC-Ag (figure 5b.7) was with very less features, with the main bands being observed at 742, 1367, 1438, and 1637 cm^{-1} (Classen et al., 2007). The broad band in the region 3450 cm^{-1} was attributed to OH stretching vibration, 1637 cm^{-1} to symmetric stretching vibration of COO^- group while the band at 1438 cm^{-1} was attributed to asymmetric stretching of C-O group and 1367 cm^{-1} to aromatic C=C stretching of trimesic acid (Chandrasekaran et al., 2015; Ruíz-Baltazar et al., 2015). The band at 740 cm^{-1} was attributed to Fe-O vibrations of iron oxide suggesting the formation of IO@BTC-Ag.

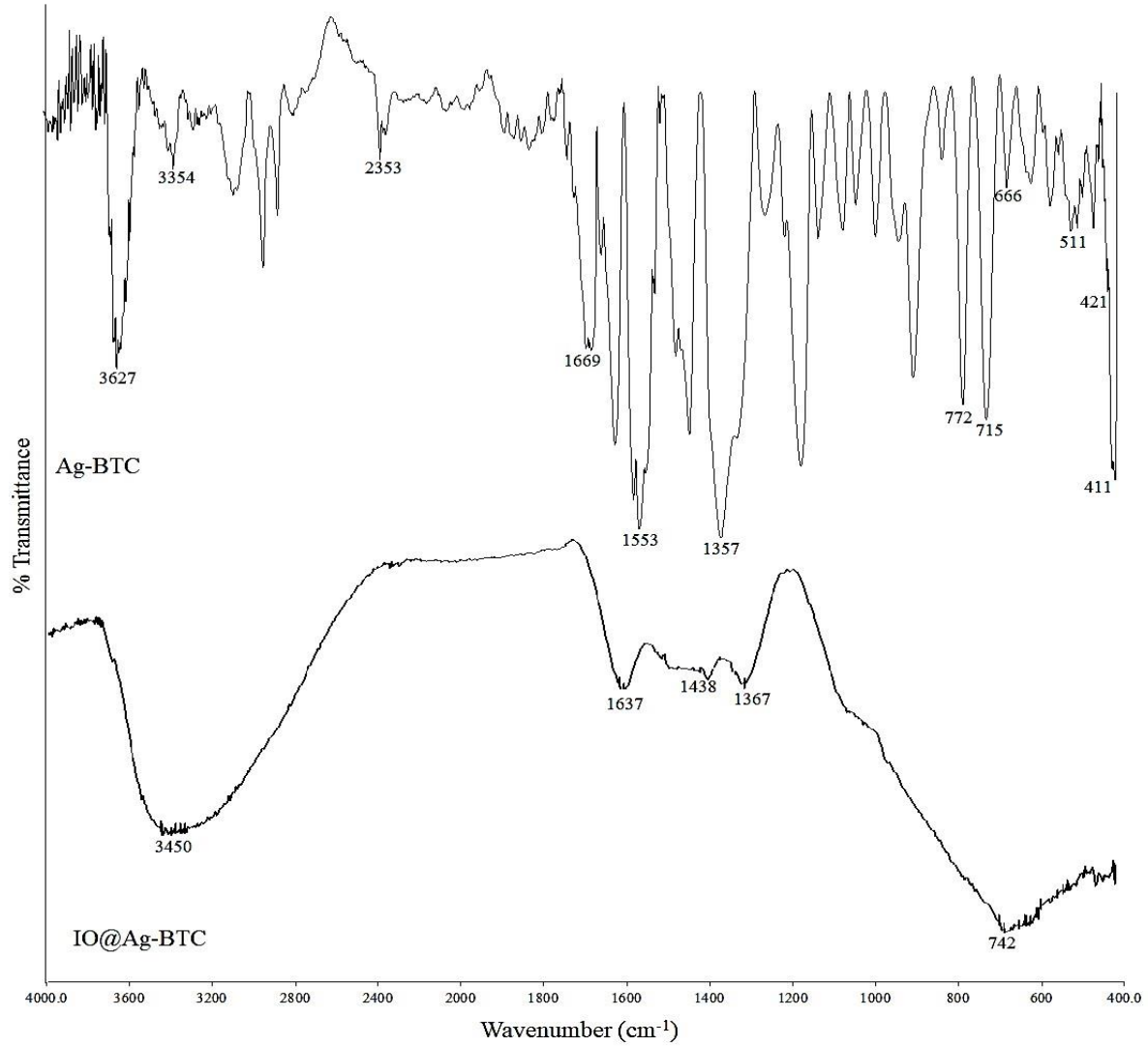

Figure 5b.7 IR spectra of Ag-BTC and IO@Ag-BTC

Raman spectroscopy analysis

The broad features in the Raman spectrum of IO@Ag-BTC (figure 5b.8) at 1359 and 1584 cm^{-1} were assigned to symmetric and asymmetric C=O stretching vibrations of carboxylate group respectively as well as ring C-C stretching modes. The scattering observed at ~745 cm^{-1} can be attributed to C-H out-of-plane bending modes of rings. The ring in plane and out of plane bending modes was observed at 450 and 385 cm^{-1} respectively. The broad band observed at 1295 cm^{-1} was assigned to O-H out-of-plane bending of carboxylic acid group(Mahalakshmi & Balachandran, 2014). The broad band centred at 683 cm^{-1} (A_1) which extended upto 745 cm^{-1} and bands at ~527 cm^{-1} (E) and ~385 cm^{-1} (T_1) were attributed to maghemite. The spectrum exhibited a sharp band at 243 cm^{-1}, attributed to the stretching vibrations of Ag–O bonds. Further the weak peaks at, 312 cm^{-1}, 541 cm^{-1} and 672 cm^{-1}

overlapping with maghemite peaks were attributed to magnetite indicating the presence of both maghemite and magnetite.

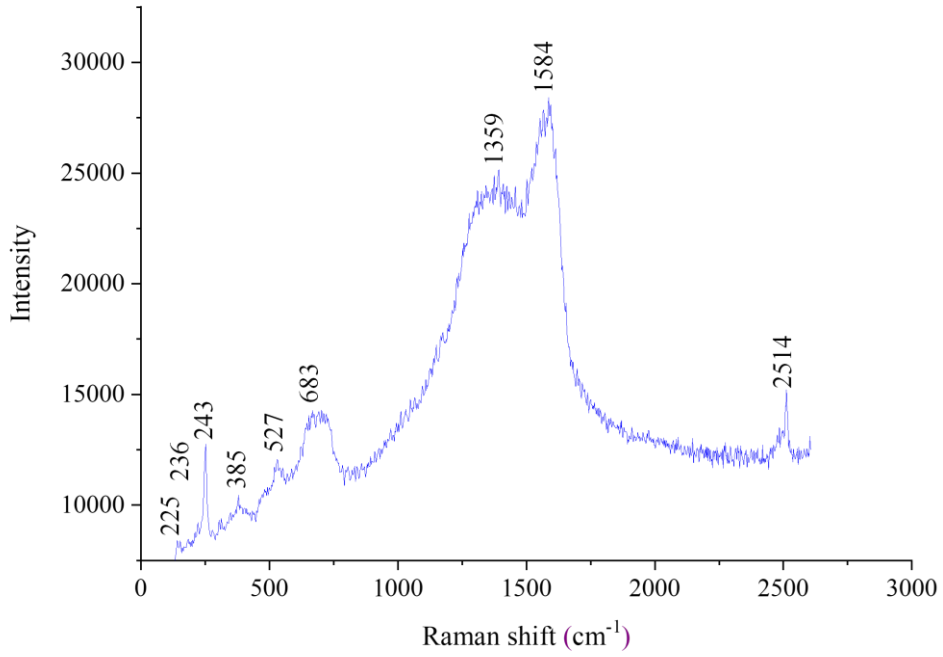

Figure 5b. 8 Raman spectrum of IO@Ag-BTC

TGA analysis

The thermogravimetric curve (figure 5b.9) of the MMOFC IO@Ag-BTC displayed a small and lineal loss of weight (~5.8%) in the interval between 30 °C and 600 °C due to evaporation of water with negligible loss of structure.

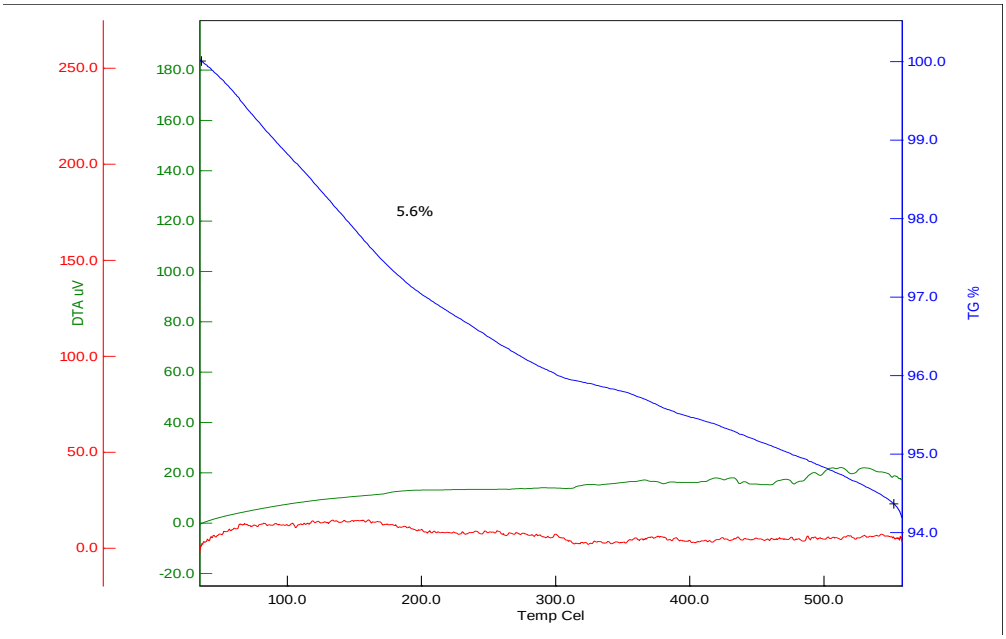

Figure 5b.9 TGA of IO@Ag-BTC

DSC analysis

The exothermic peak in the DSC thermogram may be attributed to crystallization of silver and framework reorganization followed by decomposition of BTC (figure 5b.10)

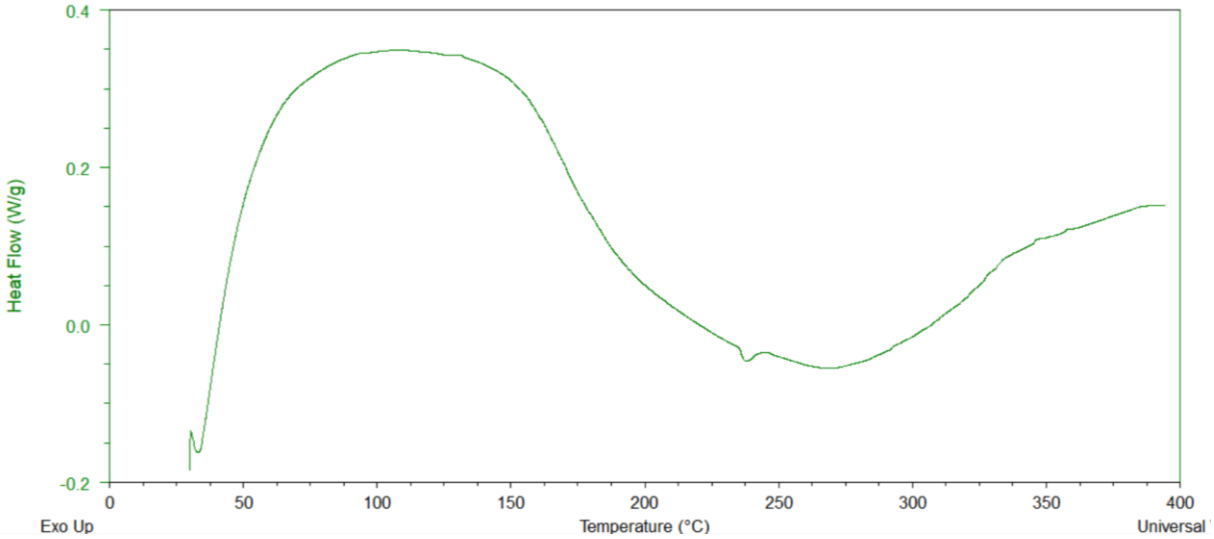

Figure 5b.10 DSC spectra of IO@Ag-BTC

VSM analysis

The magnetic property of IO@Ag-BTC MMOFC was investigated by a vibrating sample magnetometer (model 7400 with P.S 665) at ambient temperature (figure 5b.11). The absence of hysteresis loop with a saturated magnetization of 26.96 emu/g indicated the superparamagnetic nature of the MMOFC that can be magnetically separated.

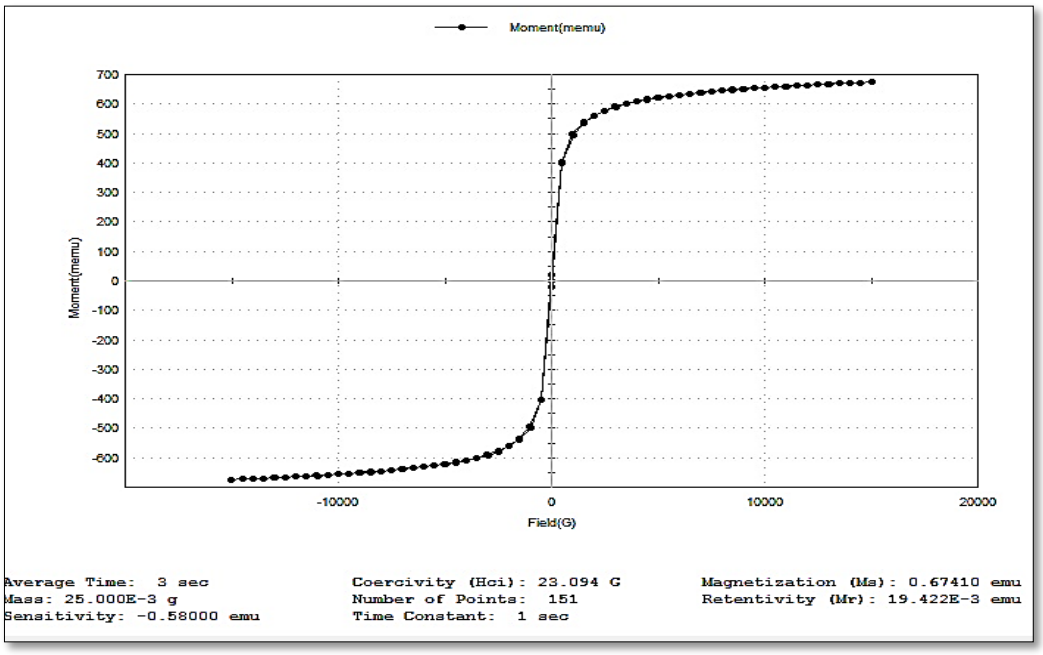

Figure 5b.11 VSM of IO@Ag-BTC

XPS analysis

The XPS deconvoluted spectra and survey spectra of Ag-BTC, IO and IO@Ag-BTC are presented in figure 5b.12, 5b.13 and 5b.14 respectively. The presence of a peak at 367.4 eV was attributed to Ag present in the bonded form in the BTC framework of Ag-BTC while the peaks at ~ 368 and 374 eV in IO@Ag-BTC was attributed to Ag^0 $3d_{5/2}$ and $3d_{3/2}$ spin orbitals respectively. The peaks at ~369 eV and 375 eV in Ag-BTC and IO@Ag-BTC respectively can be attributed to silver nanoclusters of size smaller than 10 nm (B. H. Mao et al., 2014). It was observed that nanocluster content was higher in Ag-BTC while metallic Ag content was higher in IO@Ag-BTC. This position of the band due to nanoclusters has been reported to change depending on the cluster sizes and distribution. The width observed (~1.6 eV FWHM) points to a large distribution of cluster sizes, while the metallic silver peak is positioned at the energy reported by several authors(Calderon et al., 2013).

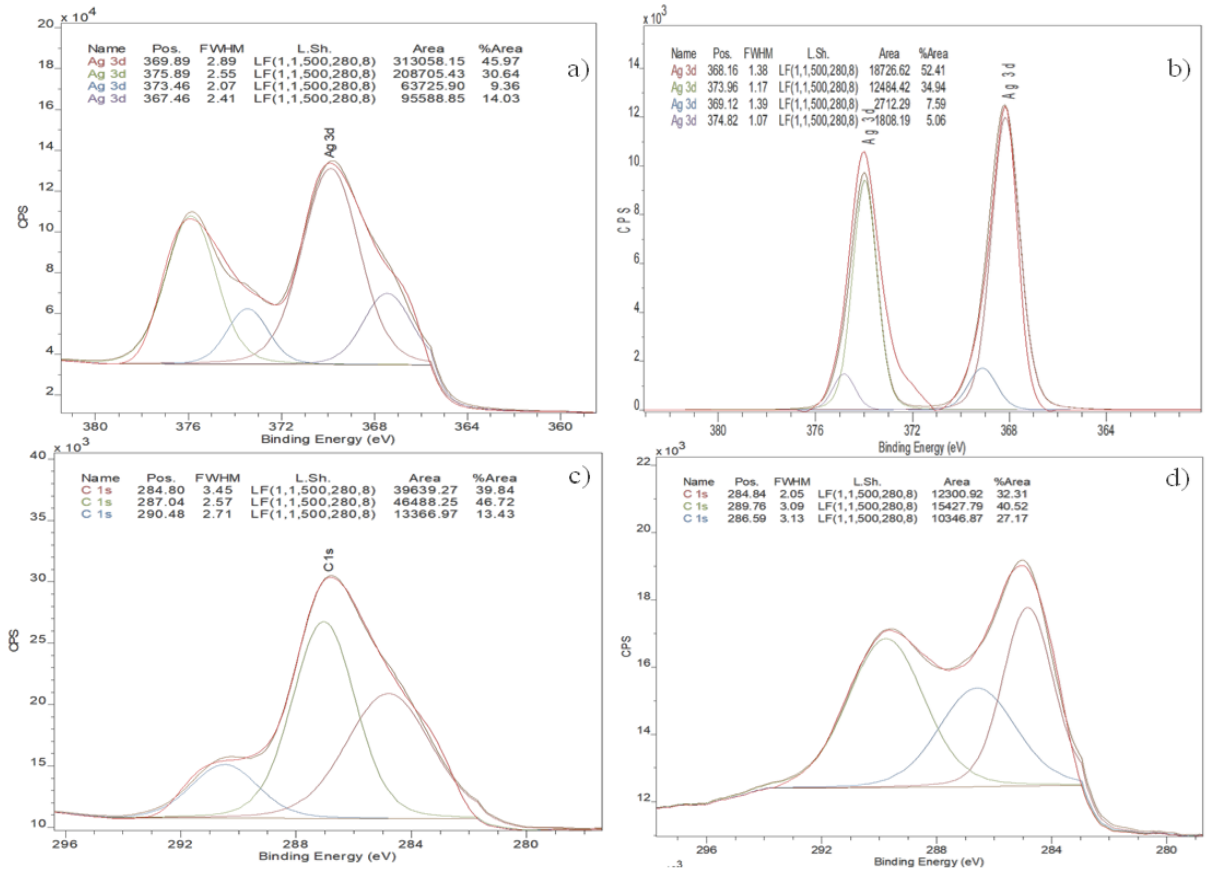

Figure 5b. 12 XPS spectra of a) Ag3d peak in Ag-BTC, b) Ag3d peak in IO@Ag-BTC c) C1s peak in Ag-BTC d) C1s peak in IO@Ag-BTC

The XPS spectra of iron in IO@Ag-BTC peaks at binding energies ~710 and 713 eV were assigned to Fe^{2+} and Fe^{3+} $2p_{3/2}$ respectively while peaks at ~723 and 726 eV were assigned to Fe^{2+} and Fe^{3+} of $Fe2p_{1/2}$ respectively. The satellite peaks corresponding to $Fe^{2+}$and

Fe^{3+}appeared in the range ~715–722 eV. The peaks observed at ~724.30 eV in iron oxide and IO@Ag-BTC corresponded to $Fe^{2+}$and ~728.93 eV to Fe^{3+}ions ($Fe2p_{1/2}$) in IO@Ag-BTC. The peaks observed at 716, 720, 729,733 eV were attributed to the satellite lines of $Fe^{2+}$and Fe^{3+}ions of $2p_{1/2}$ and $2p_{3/2}$ respectively(Bravo Sanchez et al., 2017)

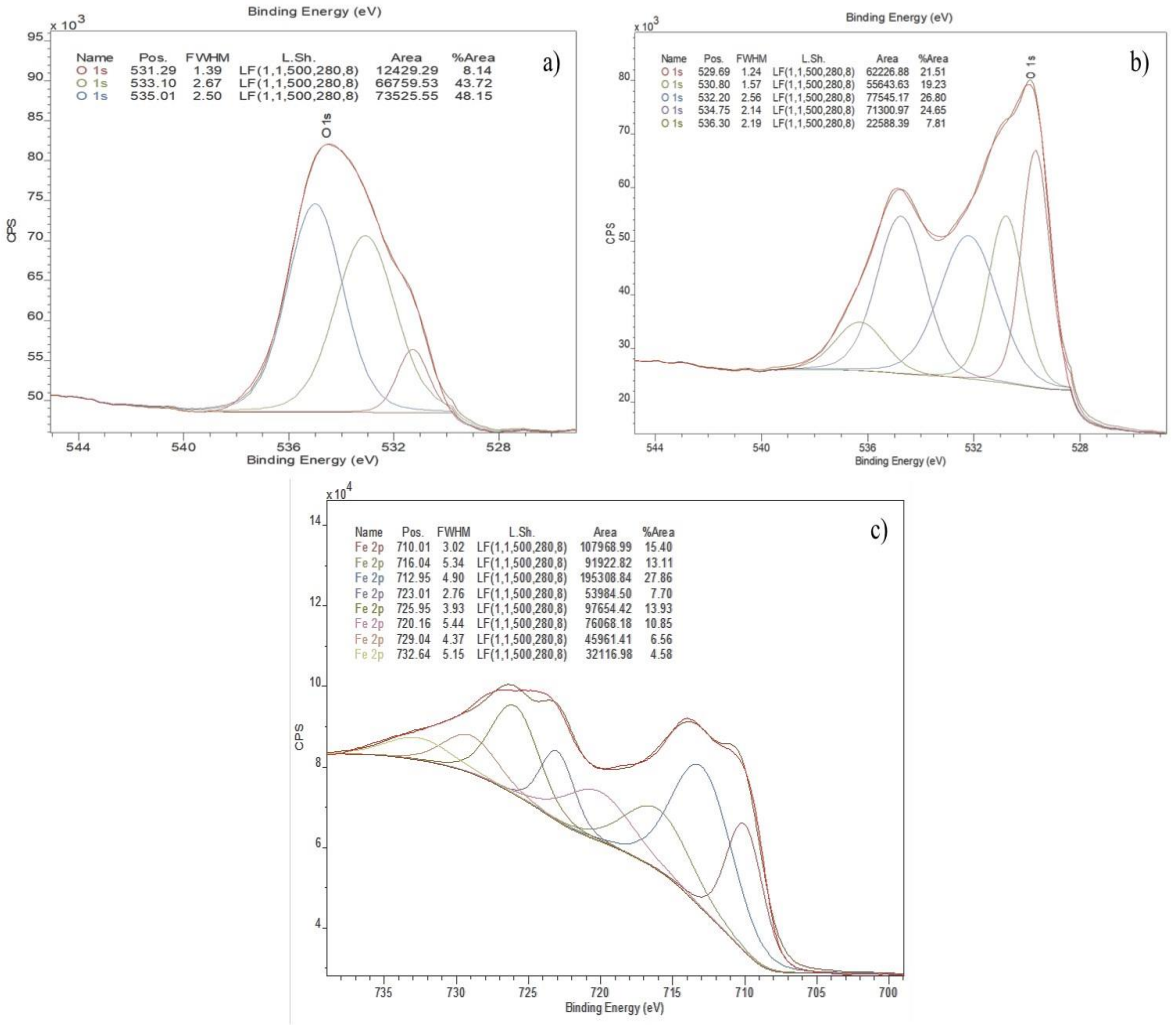

Figure 5b.13 XPS spectra of a) O1s peak in Ag-BTC b) O1s peak in IO@Ag-BTC c) Fe2p peak in IO@Ag-BTC

The C 1s spectra of Ag-BTC and IO@Ag-BTC (figure 5b.12c and 5b.12d) exhibited peaks at 284.84 eV ascribed to the aliphatic carbon. The components at binding energies ~287 eV and 290 eV clearly indicated the existence of carboxylate or carbonyl carbons. The carboxylate group gets deprotonated in alkaline medium. The deprotonated carboxylic groups stabilize silver ions (Ag^{+}) and subsequently an electron transfer from the oxygen of the trimesate anion to the silver ion (Ag^{+}) converts the silver ion to silver metal nanoparticle (Ag^{0}) which further

can interact with maghemite to form IO@Ag-BTC (Wei et al., 2017). The XPS mapping images of Ag-BTC, IO and IO@Ag-BTC are shown in figure 5b.15 (Wu et al., 2018).

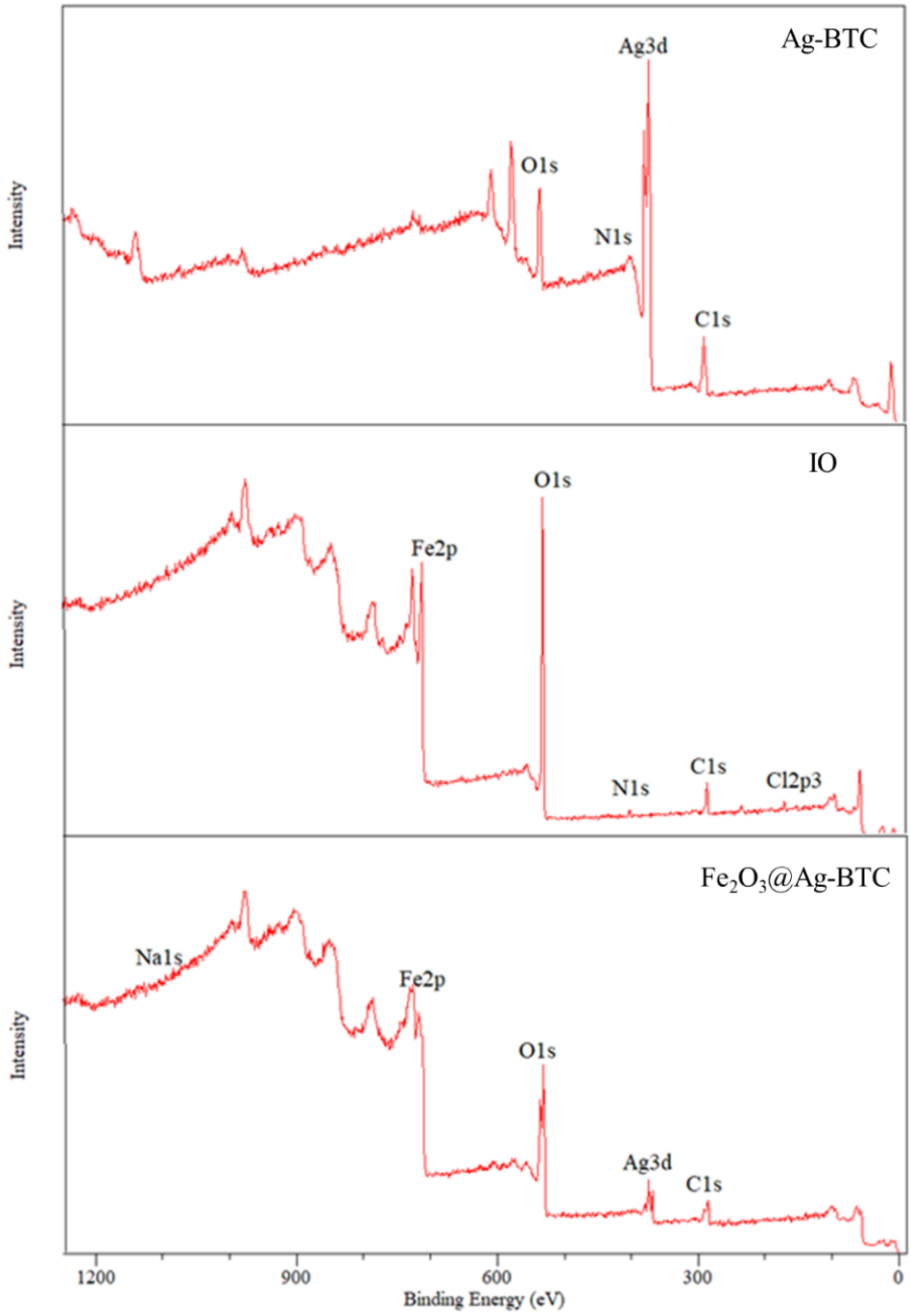

Figure 5b.14 XPS survey spectra

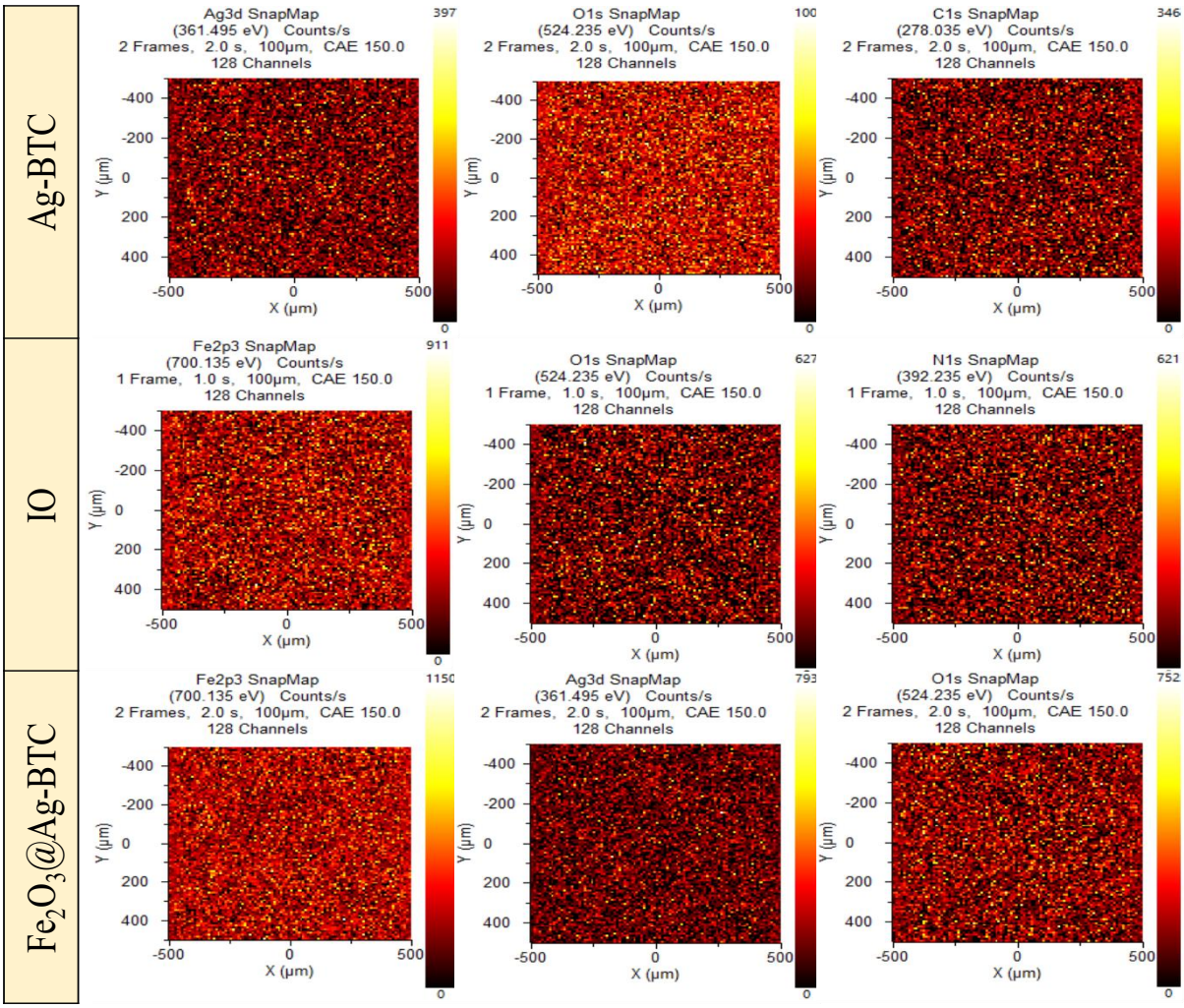

Figure 5b.15 XPS mapping images

5b.3.2. Catalytic activity

The catalytic activity of the fabricated IO@BTC-Ag MMOFC was investigated utilizing the reduction of 4-nitrophenol to 4-aminophenol with sodium borohydride as a model reaction. About 10 mg of IO@BTC-Ag MMOFC comprising 2.26 x 10^{-4} mmol silver was added to 10 mL of a solution containing 100 mg/L of 4-nitrophenol and 0.2mL of 0.1M sodium borohydride. The addition of sodium borohydride led to the solution turning yellow due to the conversion of 4-nitrophenol to nitrophenolate in alkaline conditions. The decolorization of the yellow colour after addition of the catalyst was monitored by UV- Visible spectroscopy.

The PNP exhibited an absorbance maximum at ~317 nm (figure 5b.16a), which red shifted to 400 nm in the presence of $NaBH_4$ due to the formation of 4-nitrophenolate ion in alkaline medium. On addition of IO@BTC-Ag, there was a decrease in the intensity of the absorption

peak at 400 nm with simultaneous appearance of a new peak at ~ 300 nm indicating the formation of reduction product, 4-aminophenol (4-AP).

The appearance of isosbestic point at ~320 nm, further affirmed the reduction of 4-NP to 4-AP occurred without by-product formation.

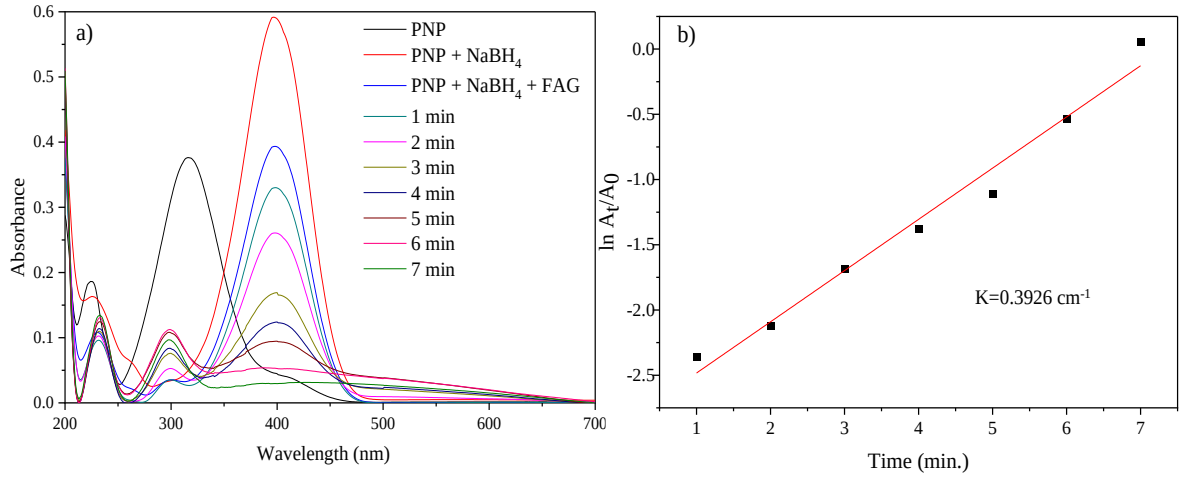

Figure 5b.16 a) UV absorption spectra of catalytic reduction of p-Nitrophenol with $NaBH_4$ in the presence of IO@Ag-BTC, b) plot of ln A_t/A_0 versus reaction time in minutes (k=0.3926 min^{-1})

The kinetics of catalytic reduction by IO@Ag-BTC was determined from UV-visible absorption spectra (figure 5b.16b). The kinetic study confirmed that the catalytic reduction followed pseudo first order kinetics in the presence of excess $NaBH_4$ with a rate constant of 0.3926 min^{-1}, calculated from the slope of the plot of $\ln A_t/A_0$ versus time (A_0 is the initial concentration of 4-nitrophenol and A_t is the concentration of 4-nitrophenol at time t).

The rate constants were comparable to those reported in the recent literature, as summarized in Table 5b.1 and required lesser amount of catalyst as compared to Fe_3O_4@GTE/Ag NPs (Veisi & Ghorbani, 2017). The rate constants with Fe_3O_4-Au Magnetic Nanocomposites(Y. Chen et al., 2018) and Au- Fe_3O_4@ MIL-100(Fe) (X. Chen et al., 2019) catalysts were higher than IO@Ag-BTC but involved the use of Au with tedious preparation methods and low reusability efficacy. However, it is difficult to compare the efficacy as the Ag loading in the reported catalysts is different and has not been reported in all the reported references in literature.

Table 5b.1 Comparison of catalytic activities for the reduction of 4-NP

Catalyst	Rate constant	Reference
$AgFe_3O_4$/ATO nano-composites	1.047 min^{-1}	(Karki et al., 2018)
Fe_3O_4-Au Magnetic Nanocomposites	0.0738 min^{-1}	(Y. Chen et al., 2018)
Fe_3O_4@GTE/Ag NPs	4.02 min^{-1}	(Veisi & Ghorbani, 2017)
Fe_3O_4@MIL-100(Fe)/Ag	2.83 min^{-1}	(Chang et al., 2020)
silver nanoparticles on 2D silica nanosheets	4.8 min^{-1}	(Yan et al., 2018)
Fe_3O_4@Pt@MIL-100(Fe)	0.38 min^{-1}	(X. Chen et al., 2019)
Fe_3O_4@Tannic acid@Au microspheres	0.38 min^{-1}	(Xiong et al., 2020)
Au- Fe_3O_4@ MIL-100(Fe)	5.53 min^{-1}	(X. Chen et al., 2019)
Ag NPs@ MOF-199 s/CCFs	0.145 min^{-1}	(Duan et al., 2019)
MAA- Fe_3O_4@ Pt/MIL-100(Fe)	2.58 min^{-1}	(H. Zhang et al., 2014)
IO@Ag-BTC	0.39 min^{-1}	This work

5b.3.3 Plausible mechanism

Ag^+ ions get reduced within the assembly of deprotonated trimesic acid network wherein the trimesic acid anion can provide electrons to the metal ions. The catalytic activity of the metal particles is due to their ability of transferring electrons from donor to acceptor.

The AgNPs in iron oxide matrix exhibit better dispersibility and smaller size than bare AgNPs, which would make the PNP molecules contact with AgNPs sufficiently and lower their interface potential barrier height. Thus, the Iron Oxide@Trimesic acid capped silver nano hetero structures show a fast electron transfer rate between the catalyst and PNP molecules.

5b.3.4 Reusability of catalyst

The main advantage of magnetic heterocatalytic system is ease of separation and reusability of the catalysts. Therefore, the reusability of IO@Ag-BTC was further investigated. The reusability was tested by separating the catalyst from solution using magnet followed by washing with water twice and drying the catalyst at 100^{o}C in oven for 2 h. Then the catalyst was reused for the next cycle.

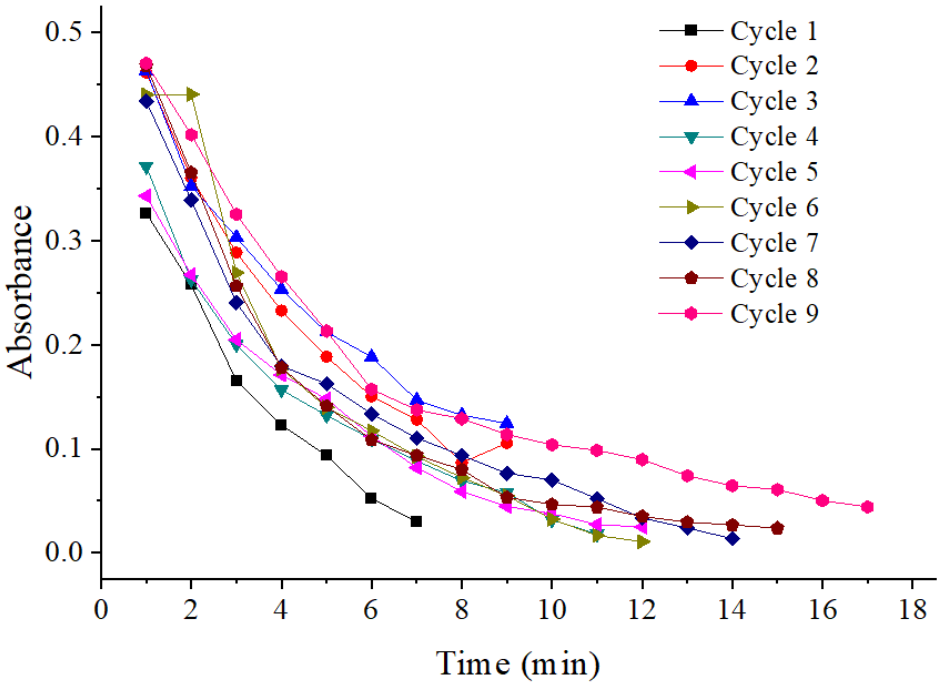

Figure 5b.17 Reusability of catalyst Cycle 1-9 after cycle 1,2,3 and 4

Figure 5b.17 shows the catalyst efficiency against time required for the reduction for particular cycle number. It can be seen that the reduction time was 7 min upto 4th cycle which increased to 8, 15, 20 and 30 min in 5th, 8th, 9th and 10th cycles respectively. The morphology of the catalysts after each cycle and the silver content was examined by SEM-EDX analysis. After 4 runs, the Ag content was reduced by 4.08 weight % (figure 5b.18).

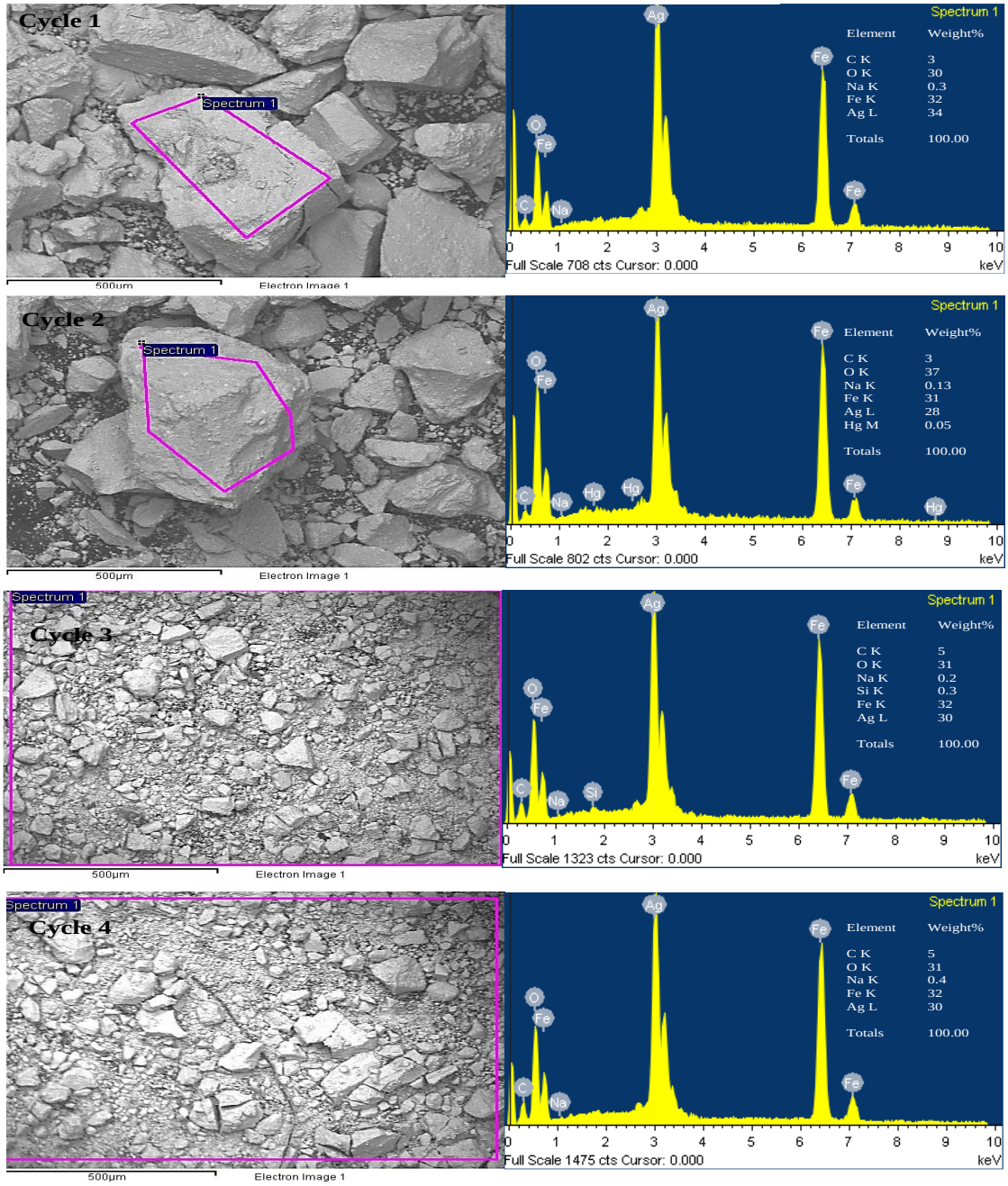

Figure 5b.18 Reusability of catalyst Cycle 1-9 and EDAX images after cycle 1,2,3 and 4

5b.4 Conclusions

In this study we developed an effective two-step method to synthesize IO@Ag-BTC MMOFCs comprising of highly dispersed AgNPs. The Ag nanoparticles were immobilized in the framework by the in-situ reduction of Ag^{+} ions. The fabricated Iron Oxide@Trimesic acid capped silver nano hetero structures were characterized by UV –Visible spectroscopy, FT-IR, Raman, SEM-EDX, TEM, SAED and XPS techniques. The fabricated MMOFCs were pseudospherical and rod shaped. IO@Ag-BTC as a facile cost effective MMOFC proved to

be a promising recoverable heterogeneous catalyst for reduction of nitrophenol with low catalyst loading.

5b.5 References

Bravo Sanchez, M., Huerta-Ruelas, J. A., Cabrera-German, D., & Herrera-Gomez, A. (2017). Composition assessment of ferric oxide by accurate peak fitting of the Fe2p photoemission spectrum. *Surface and Interface Analysis*. https://doi.org/10.1002/sia.6124

Calderon, V. S., Galindo, R. E., Benito, N., Palacio, C., Cavaleiro, A., & Carvalho, S. (2013). Ag+ release inhibition from ZrCN-Ag coatings by surface agglomeration mechanism: Structural characterization. *Journal of Physics D: Applied Physics*. https://doi.org/10.1088/0022-3727/46/32/325303

Chandrasekaran, S., Hur, H., & Kim, J. (2015). photoelectrochemical water splitting †. *RSC Advances*, *5*, 29159–29166. https://doi.org/10.1039/C5RA02934A

Chang, S., Liu, C., Sun, Y., Yan, Z., Zhang, X., Hu, X., & Zhang, H. (2020). Fe_3O_4 Nanoparticles Coated with Ag-Nanoparticle-Embedded Metal–Organic Framework MIL-100(Fe) for the Catalytic Reduction of 4-Nitrophenol . *ACS Applied Nano Materials*. https://doi.org/10.1021/acsanm.9b02415

Chen, D., Qu, Z., Sun, Y., Gao, K., & Wang, Y. (2013). Identification of reaction intermediates and mechanism responsible for highly active HCHO oxidation on Ag/MCM-41 catalysts. *Applied Catalysis B: Environmental*, *142–143*, 838–848. https://doi.org/https://doi.org/10.1016/j.apcatb.2013.06.025

Chen, X., Zhang, Y., Zhao, Y., Wang, S., Liu, L., Xu, W., Guo, Z., Wang, S., Liu, Y., & Zhang, J. (2019). Encapsulating Pt Nanoparticles through Transforming Fe_3O_4 into MIL-100(Fe) for Well-Defined Fe_3O_4@Pt@MIL-100(Fe) Core–Shell Heterostructures with Promoting Catalytic Activity. *Inorganic Chemistry*, *58*(18), 12433–12440. https://doi.org/10.1021/acs.inorgchem.9b02114

Chen, Y., Zhang, Y., Kou, Q., Liu, Y., Han, D., Wang, D., Sun, Y., Zhang, Y., Wang, Y., Lu, Z., Chen, L., Yang, J., & Xing, S. G. (2018). Enhanced catalytic reduction of 4-nitrophenol driven by Fe_3O_4-Au magnetic nanocomposite interface engineering: From facile preparation to recyclable application. *Nanomaterials*.

https://doi.org/10.3390/nano8050353

Classen, T., Lingenfelder, M., Wang, Y., Chopra, R., Virojanadara, C., Starke, U., Costantini, G., Fratesi, G., Fabris, S., De Gironcoli, S., Baroni, S., Haq, S., Raval, R., & Kern, K. (2007). Hydrogen and coordination bonding supramolecular structures of trimesic acid on Cu(110). *Journal of Physical Chemistry A*. https://doi.org/10.1021/jp076037o

Daou, T. J., Grenèche, J. M., Pourroy, G., Buathong, S., Derory, A., Ulhaq-Bouillet, C., Donnio, B., Guillon, D., & Begin-Colin, S. (2008). Coupling agent effect on magnetic properties of functionalized magnetite-based nanoparticles. *Chemistry of Materials*. https://doi.org/10.1021/cm801405n

Dong, Z., Le, X., Li, X., Zhang, W., Dong, C., & Ma, J. (2014). Silver nanoparticles immobilized on fibrous nano-silica as highly efficient and recyclable heterogeneous catalyst for reduction of 4-nitrophenol and 2-nitroaniline. *Applied Catalysis B: Environmental*, *158–159*, 129–135. https://doi.org/https://doi.org/10.1016/j.apcatb.2014.04.015

Duan, C., Liu, C., Meng, X., Lu, W., & Ni, Y. (2019). Fabrication of carboxymethylated cellulose fibers supporting Ag NPs@MOF-199s nanocatalysts for catalytic reduction of 4-nitrophenol. *Applied Organometallic Chemistry*, *33*(5), e4865. https://doi.org/https://doi.org/10.1002/aoc.4865

Gonen, S., Lori, O., Fleker, O., & Elbaz, L. (2019). Electrocatalytically Active Silver Organic Framework: Ag(I)-Complex Incorporated in Activated Carbon. *ChemCatChem*. https://doi.org/10.1002/cctc.201901604

Hossein Zadeh, M., Keramati, N., & Mehdipour Ghazi, M. (2019). The effect of solvents on photocatalytic activity of Fe-BTC metal organic framework obtained via sonochemical method. *Inorganic and Nano-Metal Chemistry*, *49*(12), 448–454. https://doi.org/10.1080/24701556.2019.1661455

Huang, R. W., Zhu, Y., Zang, S. Q., & Zhang, M. L. (2013). Construction of silver-organic framework with silver rods of repeated Ag-triangle units: Synthesis, structure, and properties. *Inorganic Chemistry Communications*. https://doi.org/10.1016/j.inoche.2013.04.006

Islam, D. A., Chakraborty, A., & Acharya, H. (2016). Fluorescent silver nanoclusters (Ag

NCs) in the metal-organic framework MIL-101(Fe) for the catalytic hydrogenation of 4-nitroaniline. *New Journal of Chemistry*, *40*(8), 6745–6751. https://doi.org/10.1039/c6nj00296j

Kamal, S., & Yang, T. C. K. (2021). A silver trimesate organic framework as an ultrasensitive surface-enhanced Raman scattering substrate for detection of various organic pollutants. *Microchemical Journal*, *163*(December 2020), 105896. https://doi.org/10.1016/j.microc.2020.105896

Karki, H. P., Ojha, D. P., Joshi, M. K., & Kim, H. J. (2018). Effective reduction of p-nitrophenol by silver nanoparticle loaded on magnetic Fe3O4/ATO nano-composite. *Applied Surface Science*, *435*, 599–608. https://doi.org/https://doi.org/10.1016/j.apsusc.2017.11.166

Kurtan, U., Amir, M., Yıldız, A., & Baykal, A. (2016). Synthesis of magnetically recyclable MnFe2O4@SiO2@Ag nanocatalyst: Its high catalytic performances for azo dyes and nitro compounds reduction. *Applied Surface Science*, *376*, 16–25. https://doi.org/https://doi.org/10.1016/j.apsusc.2016.02.120

Link, S., & El-Sayed, M. A. (1999). Spectral Properties and Relaxation Dynamics of Surface Plasmon Electronic Oscillations in Gold and Silver Nanodots and Nanorods. *Journal of Physical Chemistry B*. https://doi.org/10.1021/jp9917648

Liu, Xianchun, Jin, R., Chen, D., Chen, L., Xing, S., Xing, H., Xing, Y., & Su, Z. (2015). In situ assembly of monodispersed Ag nanoparticles in the channels of ordered mesopolymers as a highly active and reusable hydrogenation catalyst. *J. Mater. Chem. A*, *3*(8), 4307–4313. https://doi.org/10.1039/C4TA06049K

Liu, Xiang, Cheng, H., & Cui, P. (2014). Catalysis by silver nanoparticles/porous silicon for the reduction of nitroaromatics in the presence of sodium borohydride. *Applied Surface Science*, *292*, 695–701. https://doi.org/https://doi.org/10.1016/j.apsusc.2013.12.036

Mahalakshmi, G., & Balachandran, V. (2014). FT-IR and FT-Raman spectra, normal coordinate analysis and ab initio computations of Trimesic acid. *Spectrochimica Acta - Part A: Molecular and Biomolecular Spectroscopy*, *124*, 535–547. https://doi.org/10.1016/j.saa.2014.01.061

Mao, B. H., Chang, R., Shi, L., Zhuo, Q. Q., Rani, S., Liu, X. S., Tyo, E. C., Vajda, S., Wang,

S. D., & Liu, Z. (2014). A near ambient pressure XPS study of subnanometer silver clusters on Al2O3 and TiO2 ultrathin film supports. *Physical Chemistry Chemical Physics*. https://doi.org/10.1039/c4cp02325k

Mao, Q., Shi, S., & Wang, H. (2015). Biomimetic Nanowire Structured Hydrogels as Highly Active and Recyclable Catalyst Carriers. *ACS Sustainable Chemistry & Engineering*, *3*(9), 1915–1924. https://doi.org/10.1021/acssuschemeng.5b00482

Meteku, B. E., Huang, J., Zeng, J., Subhan, F., Feng, F., Zhang, Y., Qiu, Z., Aslam, S., Li, G., & Yan, Z. (2020). Magnetic metal–organic framework composites for environmental monitoring and remediation. In *Coordination Chemistry Reviews*. https://doi.org/10.1016/j.ccr.2020.213261

Naik, B., Hazra, S., Prasad, V. S., & Ghosh, N. N. (2011). Synthesis of Ag nanoparticles within the pores of SBA-15: An efficient catalyst for reduction of 4-nitrophenol. *Catalysis Communications*, *12*(12), 1104–1108. https://doi.org/https://doi.org/10.1016/j.catcom.2011.03.028

Naik, B., Prasad, V. S., & Ghosh, N. N. (2012). Preparation of Ag nanoparticle loaded mesoporous γ-alumina catalyst and its catalytic activity for reduction of 4-nitrophenol. *Powder Technology*, *232*, 1–6. https://doi.org/https://doi.org/10.1016/j.powtec.2012.07.052

Nariya, P., Das, M., Shukla, F., & Thakore, S. (2020). Synthesis of magnetic silver cyclodextrin nanocomposite as catalyst for reduction of nitro aromatics and organic dyes. *Journal of Molecular Liquids*, *300*, 112279. https://doi.org/https://doi.org/10.1016/j.molliq.2019.112279

Nguyen, T.-D., Dang, C.-H., & Mai, D.-T. (2018). Biosynthesized AgNP capped on novel nanocomposite 2-hydroxypropyl-β-cyclodextrin/alginate as a catalyst for degradation of pollutants. *Carbohydrate Polymers*, *197*, 29–37. https://doi.org/https://doi.org/10.1016/j.carbpol.2018.05.077

Oveisi, A. R., Khorramabadi-Zad, A., & Daliran, S. (2016). Iron-based metal-organic framework, Fe(BTC): An effective dual-functional catalyst for oxidative cyclization of bisnaphthols and tandem synthesis of quinazolin-4(3H)-ones. *RSC Advances*, *6*(2), 1136–1142. https://doi.org/10.1039/c5ra19013d

Panda, S. K., Chakraborti, S., & Basu, R. N. (2018). Size and shape dependences of the colloidal silver nanoparticles on the light sources in photo-mediated citrate reduction technique. *Bulletin of Materials Science*. https://doi.org/10.1007/s12034-018-1609-z

Rekha, C. R., Nayar, V. U., & Gopchandran, K. G. (2018). Synthesis of highly stable silver nanorods and their application as SERS substrates. *Journal of Science: Advanced Materials and Devices*. https://doi.org/10.1016/j.jsamd.2018.03.003

Rivera-Torrente, M., Filez, M., Hardian, R., Reynolds, E., Seoane, B., Coulet, M. V., Oropeza Palacio, F. E., Hofmann, J. P., Fischer, R. A., Goodwin, A. L., Llewellyn, P. L., & Weckhuysen, B. M. (2018). Metal-Organic Frameworks as Catalyst Supports: Influence of Lattice Disorder on Metal Nanoparticle Formation. *Chemistry - A European Journal*. https://doi.org/10.1002/chem.201800694

Ruíz-Baltazar, A., Esparza, R., Rosas, G., & Pérez, R. (2015). Effect of the Surfactant on the Growth and Oxidation of Iron Nanoparticles. *Journal of Nanomaterials*. https://doi.org/10.1155/2015/240948

Selvakannan, P. R., Mantri, K., Tardio, J., & Bhargava, S. K. (2013). High surface area Au–SBA-15 and Au–MCM-41 materials synthesis: Tryptophan amino acid mediated confinement of gold nanostructures within the mesoporous silica pore walls. *Journal of Colloid and Interface Science*, *394*, 475–484. https://doi.org/https://doi.org/10.1016/j.jcis.2012.12.008

Veisi, H., & Ghorbani, F. (2017). Iron oxide nanoparticles coated with green tea extract as a novel magnetite reductant and stabilizer sorbent for silver ions: Synthetic application of Fe3O4@green tea/Ag nanoparticles as magnetically separable and reusable nanocatalyst for reduction of 4-. *Applied Organometallic Chemistry*, *31*(10), 1–6. https://doi.org/10.1002/aoc.3711

Wei, F. H., Chen, D., Liang, Z., Zhao, S. Q., & Luo, Y. (2017). Synthesis and characterization of metal-organic frameworks fabricated by microwave-assisted ball milling for adsorptive removal of Congo red from aqueous solutions. *RSC Advances*. https://doi.org/10.1039/c7ra09243a

Wu, P., Xia, L., Liu, Y., Wu, J., Chen, Q., & Song, S. (2018). Simultaneous Sorption of Arsenate and Fluoride on Calcined Mg–Fe–La Hydrotalcite-Like Compound from Water. *ACS Sustainable Chemistry & Engineering*, *6*(12), 16287–16297.

https://doi.org/10.1021/acssuschemeng.8b03209

Xiong, L. L., Huang, R., Chai, H. H., Yu, L., & Li, C. M. (2020). Facile synthesis of Fe3O4@Tannic Acid@Au nanocomposites as a catalyst for 4-nitrophenol and methylene blue removal. *ACS Omega*. https://doi.org/10.1021/acsomega.0c02347

Yan, Z., Fu, L., Zuo, X., & Yang, H. (2018). Green assembly of stable and uniform silver nanoparticles on 2D silica nanosheets for catalytic reduction of 4-nitrophenol. *Applied Catalysis B: Environmental*. https://doi.org/10.1016/j.apcatb.2017.12.040

Yin, X. J., & Zhu, L. G. (2019). High-efficiency photocatalytic performance and mechanism of silver-based metal-organic framework. *Journal of Materials Research*, *34*(6), 991–998. https://doi.org/10.1557/jmr.2018.507

Zhang, H., Qi, S., Niu, X., Hu, J., Ren, C., Chen, H., & Chen, X. (2014). Metallic nanoparticles immobilized in magnetic metal–organic frameworks: preparation and application as highly active{,} magnetically isolable and reusable catalysts. *Catal. Sci. Technol.*, *4*(9), 3013–3024. https://doi.org/10.1039/C4CY00072B

Zhang, X., Qu, Z., Yu, F., & Wang, Y. (2013). High-temperature diffusion induced high activity of SBA-15 supported Ag particles for low temperature CO oxidation at room temperature. *Journal of Catalysis*, *297*, 264–271. https://doi.org/https://doi.org/10.1016/j.jcat.2012.10.019

Zhao, X., Liu, S., Tang, Z., Niu, H., Cai, Y., Meng, W., Wu, F., & Giesy, J. P. (2015). Synthesis of magnetic metal-organic framework (MOF) for efficient removal of organic dyes from water. *Scientific Reports*, *5*(1), 11849. https://doi.org/10.1038/srep11849